Numerical Investigation of the Mechanical Properties of 3D Printed PLA Scaffold

Zainal Abidin[1], Irfan Ghani Fadhlurrahman[1], Imam Akbar[1], Risky Utama Putra[1], Akbar Teguh Prakoso[1], M. Zahri Kadir[1], Astuti Astuti [1], Ardiyansyah Syahrom[2,3], Muhammad Imam Ammarullah[4], J. Jamari[4], Hasan Basri[1*]

[1]*Department of Mechanical Engineering, Faculty of Engineering, Universitas Sriwijaya, Indralaya, Ogan Ilir, Indonesia.*
[2]*Applied Mechanics and Design, School of Mechanical Engineering, Faculty of Engineering, Universiti Teknologi Malaysia 81310 UTM Johor Bahru, Malaysia.*
[3]*Medical Devices and Technology Centre (MEDiTEC), Institute of Human Centred and Engineering (iHumEn), Universiti Teknologi Malaysia, 81310 UTM Johor Bahru, Malaysia.*
[4]*Department of Mechanical Engineering, Faculty of Engineering, Diponegoro University, Tembalang, Semarang 50275, Central Java, Indonesia*
[*]*Corresponding author. Email: hasan_basri@unsri.ac.id*

ABSTRACT
This study aims to determine the dimensional accuracy and porosity of polylactic acid scaffold using 3D printing and the value of the effective elastic modulus. The main contribution of this research is to obtain the most suitable scaffold porosity for use as cancellous bone implants. It was obtained by comparing the dimensions and porosity of the printed scaffold with the CAD model and its effective modulus of elasticity with the cancellous bone. The 3D printing machine makes four scaffolds with varying porosity and one scaffold with 0% porosity. Scaffold dimensions were measured using a caliper. Measuring the volume of solids using a measuring cup and ethanol gives a porosity value, while as a benchmark for the total volume of the scaffold using 0% porosity. Computer simulation with MSC Marc software produces the effective modulus of elasticity. Scaffold with porosity variants of 42.9% and 58.1% showed that the results of the printed scaffold were perfect, while the porosity of 22.3% and 73.4% gave wrong impressions because they had too small pores or features. On the other hand, scaffolds with porosity of 58.1% and 73.4% had adequate elastic modulus corresponding to the span of cancellous bone. It was concluded that the porosity of the 58.1% scaffold was the best for use as a cancellous bone implant with accurate fabrication results.

Keywords: *polylactic acid, porosity, scaffold, cancellous bone, modulus of elasticity*

1. INTRODUCTION

Bone generally can fully regenerate in the event of damage, but only to a minor one. Enormous bone damage such as trauma, infections, tumors cannot regenerate fully without assistance. Therefore, tissue engineering in bone scaffolding is now a promising method of healing or replacing damaged bone.

The ideal scaffold must meet several criteria. First, the scaffold must have suitable mechanical properties, porosity, and pore size and be biocompatible. Then, the scaffold must also be produced with interconnected networks to mimic natural network architectures [1].

Among the many scaffold fabrication methods used for bone tissue engineering, three-dimensional printing is one of the newest manufacturing methods which are interesting [2][3][4]. It is a technology that can quickly create complex 3D structures. First initiated by Charles W. Hull in 1984 [5] , this technology can overcome many of the limitations of conventional fabrication methods such as electrospinning [6] and supercritical fluid foaming [7].

One of the materials that can be used as a bone scaffold and can be manufactured using 3D printing is Poly (lactic acid) (PLA) [8][9]. This material is a biodegradable polymer from renewable resources such as corn, flour, wheat, or rice. The material properties of PLA have been the subject of extensive research, including those in the biomedical field [10]. PLA is one of the most promising biodegradable polymers because it has good mechanical and biological properties such as biocompatibility and biodegradability. The degradation product of PLA is lactic acid which is non-toxic as well. It makes PLA preferred for applications in the biomedical field. Therefore, we decided to research a 3D printed PLA scaffold that focused on its elastic modulus and the machine's ability to print it.

2. MATERIALS AND METHOD

Scaffolds are based on the negatives of the Schwarz-Primitive structure (NSP), which has previously been investigated for its use for bone tissue engineering [11][12][13]. The NSP unit cell design as shown in figure 1a. There are four different porosities Φ of unit cell scaffold were considered (22.3%, 42.9%, 58.1%, 73.4%) following the range of porosity of cancellous bone structure [14][15]. The scaffolds pore size adjusted with diameters of 0.81 mm, 1.17mm, 1.4mm, and 1.72mm respectively. All scaffold models have a pore diameter of more than 0.8mm due to the FDM machine's limitations, which will make it challenging to print [4]. In addition, pore scaffold larger than 0.4mm are preferable for cell migration, proliferation and angiogenesis [16]. The unit cell scaffold was duplicated and combined then cut with a diameter of 8 mm and a height of 16 mm according ASTM D695. In addition, a solid model was created in order to morphological characteristic and simulation purposes. The cylindrical model scaffold as shown in figure 1b.

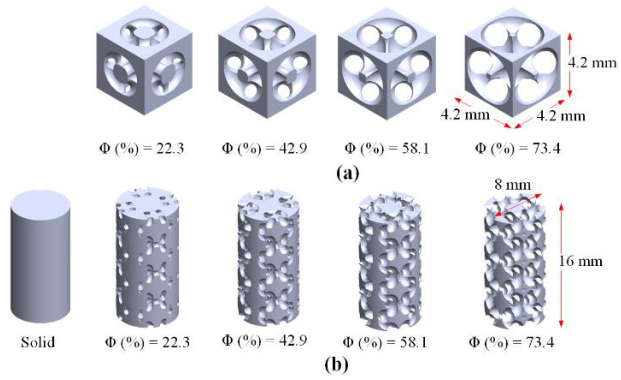

Figure 1. a) The NSP unit cell scaffold structure with porosity of 22.3, 42.9, 58.1 and 73.4 respectively; b) The unit cell was duplicated and assembled then cut with a diameter of 8 mm and a height of 16 mm according ASTM D695.

The scaffold is fabricated with natural polylactic acid (PLA) material on a Fused Deposition Modeling (FDM) 3D printer with a core XY construction. First, CAD design files were prepared with Dassault Solidworks software. Then all these CAD files were exported to stereolithography (stl) format. The exported CAD file is processed using the Ultimaker Cura 4.1.0 slicer software. In this slicer, several printing-related settings can be manipulated. A layer height of 0.1mm is used for printing this scaffold, a nozzle size of 0.2mm, a nozzle temperature of 220ºC, and a printing speed of 30mm/s. The object's orientation is made vertical because the 3D printed object has anisotropic properties [17], which means that its strength depends on the orientation of the printout. So that the printout is not contaminated by the print base using non-biodegradable PMMA [18], a raft or interface layer is used between the print object and the print base. In addition, it is set that the printer prints five scaffolds at once for more even cooling of the object. Once setup is complete, this cutter will generate a G code file for the 3D printer. Ten samples were made for each variant so that the test results data were accurate. After slicing, the G code file is sent to a USB-connected 3D printer using the Repetier Host software. This software also manages the printer firmware settings and monitors the printing process. This software can also set several parameters while printing, such as nozzle temperature and printing speed. A DIY 3D printer used is a machine is a Core XY 13 kit designed by Karya Resin 3D that has been modified in such a way as to achieve the level of precision and accuracy required to print small scaffolds, with a maximum theoretical resolution of 0.2 x 0.2 x 0.05mm.

This kit initially consists of a laser-cut plywood and acrylic frame, an acrylic (PMMA) print bed, 6mm steel rods with bimetal bushings for X and Y axes linear guides, and 8mm steel rods with bimetal bushings for the Z-axis. This machine uses an XY core configuration with 3mm GT2 belts. The Z-axis also uses a belt, unlike most 3D printers, which use a leadscrew. As the actuator, NEMA 14 stepper motors are used for the X and Y axes, and an unknown type of stepper motor for the Z-axis. This kit does not include the extruder and the electronics.

In completing the kit, an E3D titan toothed extruder is used with a NEMA 17 stepper motor as the filament drive, and then an E3D V6 hot tip is used to melt the filament the extrusion head. For electronics, an Arduino Mega 2560 and a RAMPS 1.4 board with Repetier firmware are used. These electronics will control all 3D printer functions, such as movement of the extrusion head, movement of the filament, and the melting temperature of the filament.

The modification made from this kit is to replace the bushing component with a roller whose preload can be adjusted by turning the screw on the 3D print carriage to reduce the slop that occurs due to the gap between the rod and bushing. As for the extrusion head, the nozzle is also changed from the original 0.4mm diameter to 0.2mm. The 3D printer components as shown in figure 2.

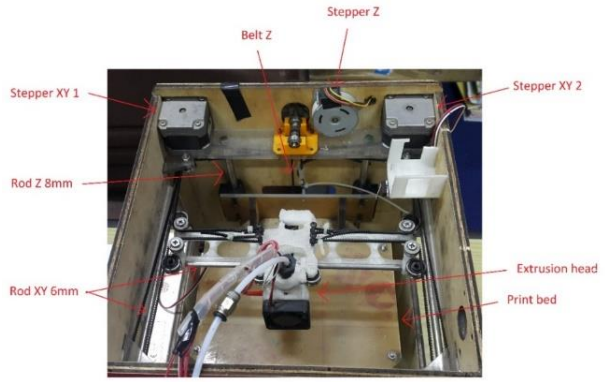

Figure 2. Top view of the coreXY 3D printer, showing the components used

After the printing is complete, the scaffolds are lifted from the print bed, removed from the raft, and cleaned of unwanted artifacts such as thin fibers and clumps of material that arise from the printing process. The specimen after printed as shown in figure 3.

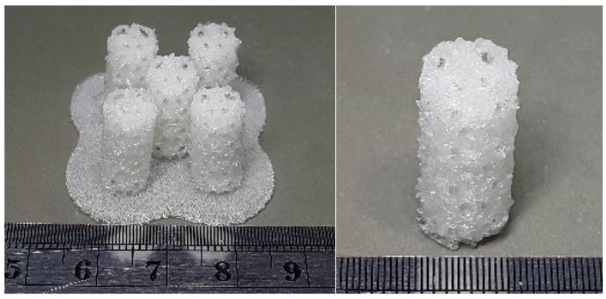

Figure 3. Print result of 45% porosity scaffold variant before and after cleaning

Measurement of the outer dimensions of the scaffolds is done by measuring the height and diameter using a caliper with an accuracy of 0.02mm.

The measurement of the porosity of the prints is carried out by measuring the volume using a measuring cup containing ethanol liquid. Ethanol is put into a measuring cup until the surface reaches a certain height, then the scaffold is inserted. From the change in surface height of ethanol, the volume of the solid part of the scaffold is known.

After the volume of the scaffold is known, the next step is to find the pore volume with Equation 1

$$V_p = V_t - V_s \quad (1)$$

Where V_p is the volume of the pore, V_s is the volume of the solid portion of the scaffold, and V_t is the total volume of both solid portion and the pore, represented by the volume of the solid (0% porosity) scaffold. After the pore volume is known, then porosity (θ) can be found by Equation 2 [19].

$$\theta = \frac{V_p}{V_t} \quad (2)$$

A compressive testing simulation was then conducted to determine the effective elastic modulus of each variant of the scaffold. The simulation is carried out in two stages: meshing with the Sharc Harpoon software and determining the material and boundary conditions, then running the simulation using the MSC Marc software.

In order to be analyzed using MSC Marc software, the .stl file, which is the surface mesh format of the Solidworks software, must first be converted to the .nas volume mesh format using the Sharc Harpoon software. The meshing process makes the object elements into a hexahedral dominant type, then pentahedral and tetrahedral, because combining these elements has better accuracy [20].

In simulating a compressive test that is close to the actual situation, the mechanical properties of polylactic acid (PLA) are inputted as follows [21][22].

Structural Properties	: Elastic-Plastic Isotropic
Young's Modulus	: 2300 MPa
Poisson's Ratio	: 0.42
Mass Density	: $1.24e^{-6}$ kg/mm^3
Yield Stress	: 35.9 MPa

Boundary conditions in the simulation are made similar to an experimental compressive test, where the upper side of the specimen is given a displacement load as a simulation of the movement of the upper plate in the experimental testing rig. The macroscopic compression strain limit of 30% was chosen for the scope of this study since plasticity is predicted to occur within the specified plastic strain range. In addition, the underside of the specimen in the opposite direction of compression load is given zero displacements in the Y or vertical direction. The schematic boundary condition as shown in figure 4. When finished, the file is saved in .dat format. The simulation starts by running its subroutine and .dat files using Fortran. The simulation is carried out on a personal computer with an Intel (R) Core (TM) i3-2100 @ 3.10GHz processor and 16 GB of RAM.

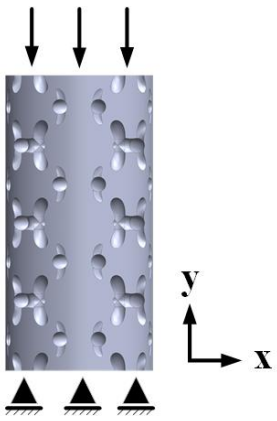

Figure 4. Schematic of boundary conditions for compressive testing

3. RESULTS AND DISCUSSION

3.1. 3D printed Scaffolds

The results of the 3D printed scaffolds can be seen in Figure 5. In general, all scaffolds have their outer dimensions and features relatively following the design. However, there are many small protrusions and strands due to the imperfect printing process for too small holes, especially on scaffolds with 22.3% porosity, holes that look closed, and features that are too small, especially on the scaffolding. Scaffold with a porosity of 73.4% is very fragile, and some even break during the printing process. It aligns with Jalil and Todo's statement [4] that the FDM printer has difficulty printing small details.

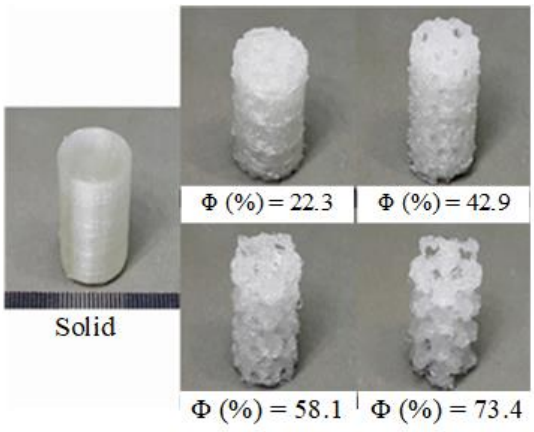

Figure 5. Scaffolds with varying porosity of 0% (left), 22.3% (top center), 42.9% (top right), 58.1% (bottom center), and 73.4% (bottom right).

Table 1. The diameter of the 3D printed scaffold in mm

Scaffold Specimen	D_S = 0%	D_S = 22.3%	D_S = 42.9%	D_S = 58.1%	D_S = 73.4%
1	7.94	8.08	7.8	8.04	7.52
2	7.86	7.9	8.1	7.8	8
3	7.92	7.8	7.94	7.74	7.7
4	7.78	8.06	7.9	7.62	7.6
5	7.86	7.86	7.74	7.72	8.2
Avg.	7.87	7.94	7.89	7.78	7.80
Avg. all	7,859				
Avg. Error	1,875%				
Max.	8.2				
Min.	7.52				

The dimensions PLA scaffolds after fabricated using FDM as tabulated in Table 1. The diameter of the scaffolds varies from the slightest 7.52 mm to the largest 8.2 mm. Most prints have a smaller diameter than the 8mm diameter of the CAD model; only four of the specimens are more significant than the 8mm diameter. The average diameter of all printed specimens is 7.85 mm, 0.15 mm smaller than the CAD model, or it can be said to have an error value of 1.9%. The belt is too flexible and its tension unbalanced, which is the leading cause of object shape distortion on the core XY 3D printers [23][24]. It explains why the dimensions of the scaffolds are less than 8 mm.

Table 2. The height of the 3D printed scaffold in mm

Scaffold Specimen	h_S = 0%	h_S = 22.3%	h_S = 42.9%	h_S = 58.1%	h_S = 73.4%
1	16.4	16.54	16.4	16.36	16.4
2	16.56	16.4	16.56	16.52	16.3
3	16.56	16.44	16.6	16.46	16.36
4	16.8	16.3	16.46	16.36	16.2
5	16.64	16.34	16.56	16.44	16.3
Avg.	16.59	16.40	16.51	16.43	16.31
Avg. all	16.45				
Avg. Error	2.81%				
Max.	16.8				
Min.	16.2				

Furthermore, the height data of all scaffold sample as tabulated in Table 2. The height of all scaffolds exceeds the dimensions of the CAD model, from 16.2mm to 16.8mm with an average height of 16.45mm, 0.45mm more remarkable than the target CAD model at 16mm, or it can be said to have an error value of 2.8%. We estimated that this is due to the use of a raft that requires a small gap (air gap) between the raft and the printed object to be separated after the print process is complete. It distorts the initial layer of the object, so it becomes taller and changes its shape. The raft, in this case, helps separate the PLA object from direct contact with the print bed made of acrylic (PMMA), which has a negative biological effect on the scaffold [25].

After measuring the dimensions, the porosity measurement is then carried out using Archimedes principles. The volume of the cast scaffold is then processed into porosity using the previously discussed equation. Volume and porosity data of the prints and their comparison with the CAD model are presented in Table 3 and Table 4.

Table 3. Volume of printed scaffolds and their comparison with the CAD models in ml

Volume	V_S = 0%	V_S = 22.3%	V_S = 42.9%	V_S = 58.1%	V_S = 73.4%
V Solid CAD	0.8	0.63	0.46	0.34	**0.21**
V Pore CAD		0.17	0.34	0.46	**0.59**
V Solid Print	0.7	0.6	0.4	0.3	**0.2**
V Pore Print		**0.1**	**0.3**	**0.4**	**0.5**

Table 4. Porosity of printed scaffolds and their comparison with CAD models

Porosity	θs = 22.3%	θs = 42.9%	θs = 58.1%	θs = 73.4%
Print (%)	14.29	42.86	57.14	71.43
CAD (%)	22.26	42.89	58.05	73.35
Error (%)	35.82	0.08	1.56	2.62

This data found that the printed solid (0% porosity) scaffold experienced a shrinkage from CAD volume of 0.8ml to 0.7ml after printing, or 12.5%. Although the height and diameter of the printed scaffold are relatively more significant than the CAD model, it is estimated that there is an invisible porosity present in the scaffold, which is the effect of layer by layer deposition on the FDM printing method. In addition, the filament lines on the bottom surface that touches the raft are not tight, causing porosity between them.

There is a significant porosity error in the scaffold with 22.3% porosity, 35.8% between the CAD and the printing. It is estimated that the small pore diameter of only 0.81mm results in an even smaller hole shape after printing. It follows the statement of Jalil and Todo [4], which states that small holes are difficult to print. In addition, inaccuracy caused by unbalanced belt tension is also thought to exacerbate this condition [23][24].

Whereas in the scaffolding with a porosity of 42.9%, 58.1%, and 73.4%, the error is relatively small, below 3%. From this, it is found that although the solid shape of the printout is not very close to the CAD model, the porosity is not much affected.

3.2. Simulation Results

The simulation of polylactic acid scaffold compressive testing using MSC Marc software produces raw data using force and displacement numbers totaling 100 increments (step) lines. This data is then processed into stress and strain data. Once processed, this data is then plotted into a graph. It has shown in Figure 6.

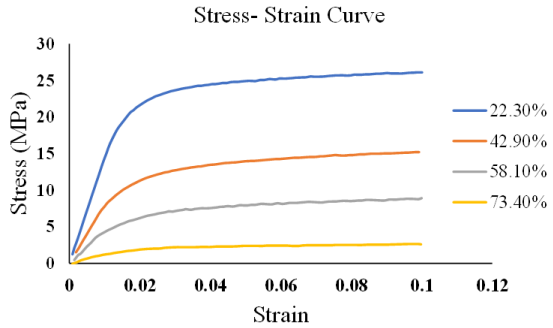

Figure 6. Compressive stress-strain curve by using finite element simulation

The stress-strain curve is presented in Figure 6. the blue line shows the scaffold with porosity of 22.3%, the red line shows the scaffold with porosity of 42.9%, the green line shows the scaffold with porosity of 58.1%, and the purple line shows the scaffold with porosity of 73.4%. This graph shows that the higher the porosity, the lower the stress and the effective elastic modulus. Also, the effective elastic modulus of each sample is then presented in the form of a bar chart to be compared with the modulus of elasticity of the cancellous bone (see Figure 7).

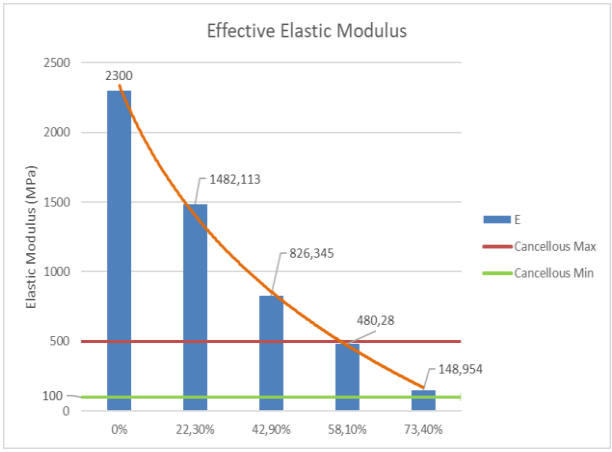

Figure 7. Elastic modulus vs porosity

These two graphs show an inversely proportional relationship between porosity and modulus of elasticity; that is, the higher the porosity means, the lower the effective elastic modulus. It is consistent with previous studies on the relationship between porosity and the modulus of elasticity [26][27][28][29]. In addition, this also shows that the scaffolds with porosity of 58.1% and 73.4% fall into the elastic modulus range of the cancellous bone between 100 - 500 MPa [30] with a nominal value of 480.28 MPa and 148,954 MPa, while the scaffolds with a porosity of 42.9%, 22.3%, and solid exceed the upper limit of 500 MPa with nominal values of 826,345 MPa, 1482,113 MPa, and 2300 MPa respectively [22]. As previously explained, the scaffold must have a modulus of elasticity close to the bone it is replacing [31]; it concludes that the scaffold which is most suitable for use when viewed from the perspective of effective elastic modulus is one with a porosity of 58.1% and 73.4%.

4. CONCLUSIONS

From the research that has been done, the following conclusions can be drawn:

1. Scaffolds with porosity of 42.9% and 58.1% are the best because their features are perfectly printed and have dimensional and porosity error values of less than 3%.
2. The effective modulus of elasticity of the scaffold with porosity of 22.3%, 42.9%, 58.1%, and 73.5% are 1482,113 MPa, 826,345 MPa, 480.28 MPa, and

149,954 MPa, respectively. Scaffolds with porosity of 58.1% and 73.4% have an effective modulus of elasticity that falls within the modulus of elasticity of cancellous bone.

3. The effective elasticity modulus of the scaffold is inversely proportional to the porosity. The higher the modulus of elasticity, the lower the porosity.
4. The polylactic acid scaffold with porosity 58.1% meets the requirements for use as bone implants.

ACKNOWLEDGMENTS

The research publication of this article was funded by the DIPA of Public Service Agency of Universitas Sriwijaya 2021. SP DIPA-023.17.2.677515/2021, On November 23, 2020. Under the Rector's Decree Number: 0023/UN9/SK.LP2M.PT/2021, On July 22, 2021. We gratefully thank the Mechanical Engineering Department, Faculty of Engineering, Universitas Sriwijaya for their strong support of this study, along with the Medical Device and Technology Center (MEDITEC), Institute of Human-Centered and Engineering (iHumEn), Universiti Teknologi Malaysia, Department of Mechanical Engineering, and State Polytechnic of Sriwijaya for their encouragement and many fruitful discussions on this research.

REFERENCES

[1] S. V. Murphy and A. Atala, "3D bioprinting of tissues and organs," *Nat. Biotechnol.*, vol. 32, no. 8, pp. 773–785, 2014, doi: 10.1038/nbt.2958.

[2] Y. Yang *et al.*, "Additive manufacturing of bone scaffolds," *Int. J. Bioprinting*, vol. 5, no. 1, pp. 1–25, 2019, doi: 10.18063/IJB.v5i1.148.

[3] L. Germain, C. A. Fuentes, A. W. van Vuure, A. des Rieux, and C. Dupont-Gillain, "3D-printed biodegradable gyroid scaffolds for tissue engineering applications," *Mater. Des.*, 2018, doi: 10.1016/j.matdes.2018.04.037.

[4] M. H. Jalil and M. Todo, "Development and Characterization of Gear Shape Porous Scaffolds Using 3D Printing Technology," *Int. J. Biosci. Biochem. Bioinforma.*, 2017, doi: 10.17706/ijbbb.2017.7.2.74-83.

[5] C. W. Hull, "Apparatus for Production of Three-Dmensonal Objects By Stereo Thography," *Patent*, 1984.

[6] Y. Li, C. T. Lim, and M. Kotaki, "Study on structural and mechanical properties of porous PLA nanofibers electrospun by channel-based electrospinning system," *Polymer (Guildf).*, 2015, doi: 10.1016/j.polymer.2014.10.073.

[7] M. Chauvet, M. Sauceau, and J. Fages, "Extrusion assisted by supercritical CO2: A review on its application to biopolymers," *J. Supercrit. Fluids*, 2017, doi: 10.1016/j.supflu.2016.05.043.

[8] T. Serra, M. A. Mateos-Timoneda, J. A. Planell, and M. Navarro, "3D printed PLA-based scaffolds: A versatile tool in regenerative medicine," *Organogenesis*. 2013, doi: 10.4161/org.26048.

[9] R. Fairag, D. H. Rosenzweig, J. L. Ramirez-Garcialuna, M. H. Weber, and L. Haglund, "Three-Dimensional Printed Polylactic Acid Scaffolds Promote Bone-like Matrix Deposition in Vitro," *ACS Appl. Mater. Interfaces*, 2019, doi: 10.1021/acsami.9b02502.

[10] D. Djidi, N. Mignard, and M. Taha, "Thermosensitive polylactic-acid-based networks," *Ind. Crops Prod.*, 2015, doi: 10.1016/j.indcrop.2014.09.035.

[11] D. Ali, "Effect of scaffold architecture on cell seeding efficiency: A discrete phase model CFD analysis," *Comput. Biol. Med.*, 2019, doi: 10.1016/j.compbiomed.2019.04.025.

[12] R. Ambu and A. E. Morabito, "Modeling, assessment, and design of porous cells based on schwartz primitive surface for bone scaffolds," *Sci. World J.*, 2019, doi: 10.1155/2019/7060847.

[13] R. Guerreiro, T. Pires, J. M. Guedes, P. R. Fernandes, and A. P. G. Castro, "On the tortuosity of TPMS scaffolds for tissue engineering," *Symmetry (Basel).*, vol. 12, no. 4, pp. 17–19, 2020, doi: 10.3390/SYM12040596.

[14] L. Polo-Corrales, M. Latorre-Esteves, and J. E. Ramirez-Vick, "Scaffold design for bone regeneration.," *J. Nanosci. Nanotechnol.*, vol. 14, no. 1, pp. 15–56, 2014, doi: 10.1166/jnn.2014.9127.

[15] J. Rouwkema, N. C. Rivron, and C. A. van Blitterswijk, "Vascularization in tissue engineering," *Trends in Biotechnology*. 2008, doi: 10.1016/j.tibtech.2008.04.009.

[16] F. S. L. Bobbert and A. A. Zadpoor, "Effects of bone substitute architecture and surface properties on cell response, angiogenesis, and structure of new bone," *Journal of Materials Chemistry B*. 2017, doi: 10.1039/c7tb00741h.

[17] J. J. Laureto and J. M. Pearce, "Anisotropic mechanical property variance between ASTM D638-14 type i and type iv fused filament fabricated specimens," *Polym. Test.*, 2018, doi: 10.1016/j.polymertesting.2018.04.029.

[18] A. Subramaniam and S. Sethuraman, "Biomedical Applications of Nondegradable

Polymers," in *Natural and Synthetic Biomedical Polymers*, 2014.

[19] P. S. Liu and G. F. Chen, "Characterization Methods," *Porous Mater.*, pp. 411–492, 2014, doi: 10.1016/b978-0-12-407788-1.00009-5.

[20] C. Veyhl, I. V. Belova, G. E. Murch, A. Öchsner, and T. Fiedler, "On the mesh dependence of non-linear mechanical finite element analysis," *Finite Elem. Anal. Des.*, vol. 46, no. 5, pp. 371–378, 2010, doi: 10.1016/j.finel.2009.12.003.

[21] J. L. Milan, J. A. Planell, and D. Lacroix, "Computational modelling of the mechanical environment of osteogenesis within a polylactic acid-calcium phosphate glass scaffold," *Biomaterials*, 2009, doi: 10.1016/j.biomaterials.2009.04.026.

[22] A. Entezari, J. Fang, A. Sue, Z. Zhang, M. V. Swain, and Q. Li, "Yielding behaviors of polymeric scaffolds with implications to tissue engineering," *Mater. Lett.*, 2016, doi: 10.1016/j.matlet.2016.07.149.

[23] T. S. S. Jayawardene, M. Nakamura, and S. Goto, "Accurate control position of belt drives under acceleration and velocity constraints," *Int. J. Control. Autom. Syst.*, 2003.

[24] A. R. Avdeev, A. A. Shvets, and I. S. Torubarov, "Investigation of Kinematics of 3D Printer Print Head Moving Systems," 2020, doi: 10.1007/978-3-030-22041-9_50.

[25] H. K. Park, M. Dujovny, C. Agner, and F. G. Diaz, "Biomechanical properties of calvarium prosthesis," *Neurol. Res.*, 2001, doi: 10.1179/016164101101198424.

[26] M. A. Sulong, I. V. Belova, A. R. Boccaccini, G. E. Murch, and T. Fiedler, "A model of the mechanical degradation of foam replicated scaffolds," *J. Mater. Sci.*, vol. 51, no. 8, pp. 3824–3835, 2016, doi: 10.1007/s10853-015-9701-x.

[27] X. C. Xia *et al.*, "Effects of porosity and pore size on the compressive properties of closed-cell Mg alloy foam," *J. Magnes. Alloy.*, vol. 1, no. 4, pp. 330–335, 2013, doi: 10.1016/j.jma.2013.11.006.

[28] R. B. Diego, J. M. Esteîlés, J. A. Sanz, J. M. García-Asnar, and M. S. Sánchez, "Polymer scaffolds with interconnected spherical pores and controlled architecture for tissue engineering: Fabrication, mechanical properties, and finite element modeling," *J. Biomed. Mater. Res. - Part B Appl. Biomater.*, 2007, doi: 10.1002/jbm.b.30683.

[29] D. Lacroix, A. Chateau, M. P. Ginebra, and J. A. Planell, "Micro-finite element models of bone tissue-engineering scaffolds," *Biomaterials*, vol. 27, no. 30, pp. 5326–5334, 2006, doi: 10.1016/j.biomaterials.2006.06.009.

[30] J. L. Williams and J. L. Lewis, "Properties and an anisotropic model of cancellous bone from the proximal tibial epiphysis," *J. Biomech. Eng.*, 1982, doi: 10.1115/1.3138303.

[31] M. I. Sabir, X. Xu, and L. Li, "A review on biodegradable polymeric materials for bone tissue engineering applications," *J. Mater. Sci.*, 2009, doi: 10.1007/s10853-009-3770-7.